

Numerical Study of Single Air Bubble Formation in Viscous Liquid

Debdip Biswas¹, Prof. Yogesh Ahire², Mr. Evan Fernandes³

¹*National Institute of Technology Calicut*

²*Sanjivani College of Engineering*

³*Indian Institute of Technology Bombay*

Synopsis

The dynamics of bubble formation in viscous liquids is a complex multiphase problem governed by the effects of buoyancy, surface tension, and viscous forces. This project numerically investigates the growth, necking, and detachment of an air bubble from a submerged nozzle. Using the `interFoam` solver in OpenFOAM v9, the study replicates the physics presented by Quan and Hua (2008). Detailed parametric studies were conducted to analyze the influence of liquid viscosity, surface tension, and gas density on the pinch-off mechanism. The simulation results, specifically, the bubble shape, neck thinning rates, pinch-off heights, and detached volumes were validated against the reference numerical data. The findings confirm that, while gas density has a negligible effect, liquid viscosity and surface tension significantly alter the power-law scaling of the neck radius, pinch-off height and the final bubble volume.

1 Introduction

The detachment of gas bubbles from a nozzle in a quiescent liquid is a fundamental process in many industrial applications, from bioreactors to chemical processing. Unlike drop breakup in inviscid fluids, which follows universal scaling laws, bubble pinch-off in viscous fluids exhibits non-universal behavior due to the significant role of viscous stresses.

Quan and Hua (2008) utilized a front-tracking finite-volume method to demonstrate that the bubble neck radius (r) scales with the time remaining to pinch-off (τ) as $r \sim \tau^\alpha$. They showed that the exponent α is not fixed but changes from approximately 0.5 to 1.0 as the liquid viscosity increases.

This report documents the migration of this research using OpenFOAM. By solving the Navier-Stokes equations with a Volume of Fluid (VOF) approach, we aim to reproduce the distinct flow regimes and quantitative relationships reported in the literature, specifically focusing on how fluid properties dictate the necking dynamics and final bubble characteristics.

2 Literature Review

The physics of bubble growth has been extensively studied over the past few decades. Oguz and Prosperetti (1993) provided seminal work on the dynamics of bubble growth and detachment from needles [3]. Their boundary-integral simulations and theoretical models elucidated the force balance between buoyancy and surface tension, identifying distinct growth regimes based on gas flow rates. Their work established the fundamental understanding that at low flow rates (quasi-static regime), the detachment is force-controlled, a concept central to verifying the force balance in the current study.

As research moved towards viscous fluids, the focus shifted to the "necking" singularity. The primary reference for this work, Quan and Hua (2008), utilized a front-tracking finite-volume method to investigate bubble necking in viscous liquids [1]. They demonstrated that the neck thinning process is non-universal. They reported that the power-law exponent α (where $r \sim \tau^\alpha$) varies from approximately 0.5 in inviscid fluids to nearly 1.0 in highly viscous fluids, challenging the idea of a single universal pinch-off mechanism.

Implementing these physics in modern CFD tools requires specific domain handling. Oshaghi et al. (2019) conducted extensive numerical investigations of bubble formation in shear-thinning liquids using OpenFOAM [4]. Their work provided critical insights for the current project, particularly with respect to the construction of the computational domain. Following their approach, this project employs a 2D axisymmetric wedge geometry generated via blockMesh, which significantly reduces computational cost while maintaining high fidelity in capturing the interface curvature during pinch-off.

3 Governing Equations

The numerical simulation employs the `interFoam` solver, which solves the Navier-Stokes equations for two incompressible, isothermal, and immiscible fluids. In this formulation, the material properties are treated as constant within each phase, varying only across the interface.

3.1 Continuity Equation

For a constant-density fluid mixture, the continuity equation is written as:

$$\frac{\partial u_j}{\partial x_j} = 0 \quad (1)$$

3.2 Momentum Equation

The transport of momentum is governed by a single equation for the mixture:

$$\frac{\partial(\rho u_i)}{\partial t} + \frac{\partial}{\partial x_j}(\rho u_j u_i) = -\frac{\partial p}{\partial x_i} + \frac{\partial}{\partial x_j}(\tau_{ij} + \tau_{t,ij}) + \rho g_i + f_{\sigma i} \quad (2)$$

where u represents the velocity vector, g_i is the gravitational acceleration, and p denotes the pressure. The terms τ_{ij} and $\tau_{t,ij}$ correspond to the viscous and turbulent stresses, respectively, while $f_{\sigma i}$ represents the surface tension force.

The mixture density ρ is computed based on the phase fraction:

$$\rho = \alpha\rho_1 + (1 - \alpha)\rho_2 \quad (3)$$

Here, α is 1 inside fluid 1 (with density ρ_1) and 0 inside fluid 2 (with density ρ_2). At the interface between the two fluids, α varies between 0 and 1.

The surface tension force, $f_{\sigma i}$, is modeled using the Continuum Surface Force (CSF) method and is calculated as:

$$f_{\sigma i} = \sigma \kappa \frac{\partial \alpha}{\partial x_i} \quad (4)$$

where σ is the surface tension constant and κ is the interface curvature. The curvature is approximated as:

$$\kappa = -\frac{\partial n_i}{\partial x_i} = -\frac{\partial}{\partial x_i} \left(\frac{\partial \alpha / \partial x_i}{|\partial \alpha / \partial x_i|} \right) \quad (5)$$

3.3 Equation for the Interface

To track the location of the interface between the two fluids, an additional transport equation for the phase fraction α is solved:

$$\frac{\partial \alpha}{\partial t} + \frac{\partial (\alpha u_j)}{\partial x_j} = 0 \quad (6)$$

This equation represents the conservation of the mixture components as they travel along the path of a fluid parcel.

The quantity α represents the Volume of Fluid (VOF) in a unit volume and is defined as follows:

$$\alpha = \begin{cases} 0 & \text{In the bubble (gas)} \\ 0 < \alpha < 1 & \text{At the interface} \\ 1 & \text{In the liquid} \end{cases} \quad (7)$$

4 Turbulence Modeling

Given the physical parameters of the problem (small capillary nozzle $R_0 = 1.35$ mm and highly viscous liquids ranging up to 3400 cP), the Reynolds number remains significantly low. The flow is dominated by viscous and surface tension forces rather than inertial fluctuations. Therefore, the simulation is performed in the **laminar** regime, and no turbulence models are activated.

5 Computational Setup

5.1 Geometry

To accurately capture the axisymmetric nature of the bubble formation, a 2D wedge geometry was employed. The domain dimensions are set to a radius of $3r_0$ and a height of $12r_0$, where $r_0 = 1.35$ mm is the nozzle radius. This size ensures that boundary effects from the walls do not influence the bubble dynamics.

5.2 Mesh

A structured hexahedral mesh was generated using the blockMesh utility. Grading was applied to refine the mesh near the nozzle exit and the axis of symmetry to resolve the high curvature of the necking region during pinch-off.

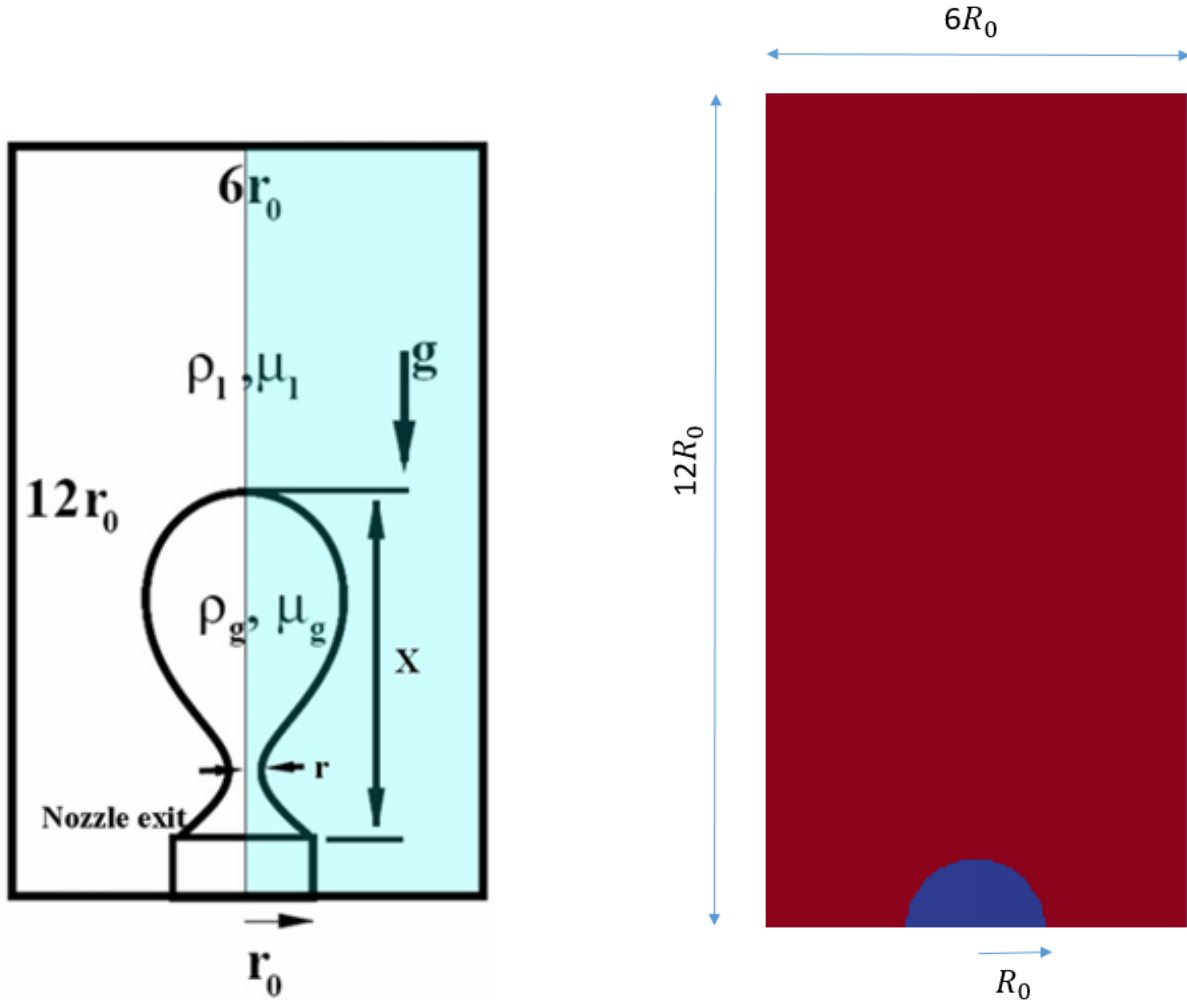


Figure 1: Problem schematic and the computational domain used for the simulation.

5.3 Boundary and Initial Conditions

The domain is initially filled with liquid ($\alpha = 1$) at rest ($\mathbf{U} = 0$). Air is injected through the inlet patch.

Table 1: Boundary Conditions

Patch	Velocity (\mathbf{U})	Pressure (p_{rgh})	Alpha
inlet	flowRateInletVelocity	fixedFluxPressure	fixedValue (0)
outlet	pressureInletOutletVelocity	totalPressure	inletOutlet
bottomWall	noSlip	fixedFluxPressure	zeroGradient
sideWall	noSlip	fixedFluxPressure	zeroGradient
front/back	wedge	wedge	wedge

5.4 Solver Selection

The `interFoam` solver was selected as it is the standard OpenFOAM solver for two incompressible, immiscible fluids using the VOF method.

5.5 Discretization Schemes

- **Time:** Euler (first order implicit)
- **Gradient:** Gauss linear
- **Divergence:** Gauss vanLeer (for alpha), Gauss linear (for velocity)
- **Laplacian:** Gauss linear corrected

5.6 Simulation Parameters

- **Max Courant Number (Co):** 0.5 (to ensure stability)
- **Time Step (ΔT):** Adjustable time stepping employed.
- **Reynolds Number (Re):** Variable depending on viscosity case (Laminar regime).

6 Implementation in OpenFOAM

6.1 Case Setup Structure

The simulation case follows the standard OpenFOAM directory structure:

- 0/: Contains initial conditions for `U`, `p_rgh`, and `alpha.water`.

- `constant/`: Contains `transportProperties` (fluid properties), `g` (gravity), `turbulenceProperties` (set to laminar).
- `system/`: Contains `blockMeshDict`, `setFieldsDict`, `controlDict`, `fvSchemes`, and `fvSolution`.

6.2 Control Dictionary

The simulation was controlled using `controlDict` with the `adjustTimeStep` feature enabled to maintain the Courant number limit. The write interval was set to a sufficiently small value (10^{-4} s) near the pinch-off event to capture the rapid topological changes.

6.3 Running Procedure

The simulations were computationally efficient due to the 2D axisymmetric wedge simplification. The entire simulation workflow can be automated using an `Allrun` script attached. The procedure consisted of the following steps:

1. **Mesh Generation:** The domain is created using `blockMesh`.
2. **Initialization:** The phase fields are initialized using `setFields`.
3. **Decomposition:** For parallel computation, the domain can be divided among processors available `decomposePar`.
4. **Solving:** The simulation is executed using the `interFoam` solver.
5. **Reconstruction:** Post-simulation, the results are compiled back into a single domain using `reconstructPar` for Post Processing in ParaView.

6.4 Total Time

Each simulation was run until the bubble detached and moved sufficiently away from the nozzle, typically requiring 1.5 to 3.0 seconds of physical time depending on the liquid viscosity.

6.5 OpenFOAM Version

All simulations were performed using OpenFOAM v9.

7 Results and Discussion

7.1 Validation of Interface Evolution

The solver was first validated against the experimental bubble shapes for an air-water system ($\mu_l \approx 1$ cP). As shown in Figure 2, the simulation (continuous blue lines) aligns precisely with the paper's simulation (dotted lines), accurately predicting the bubble volume and the distinct neck shape at pinch-off.

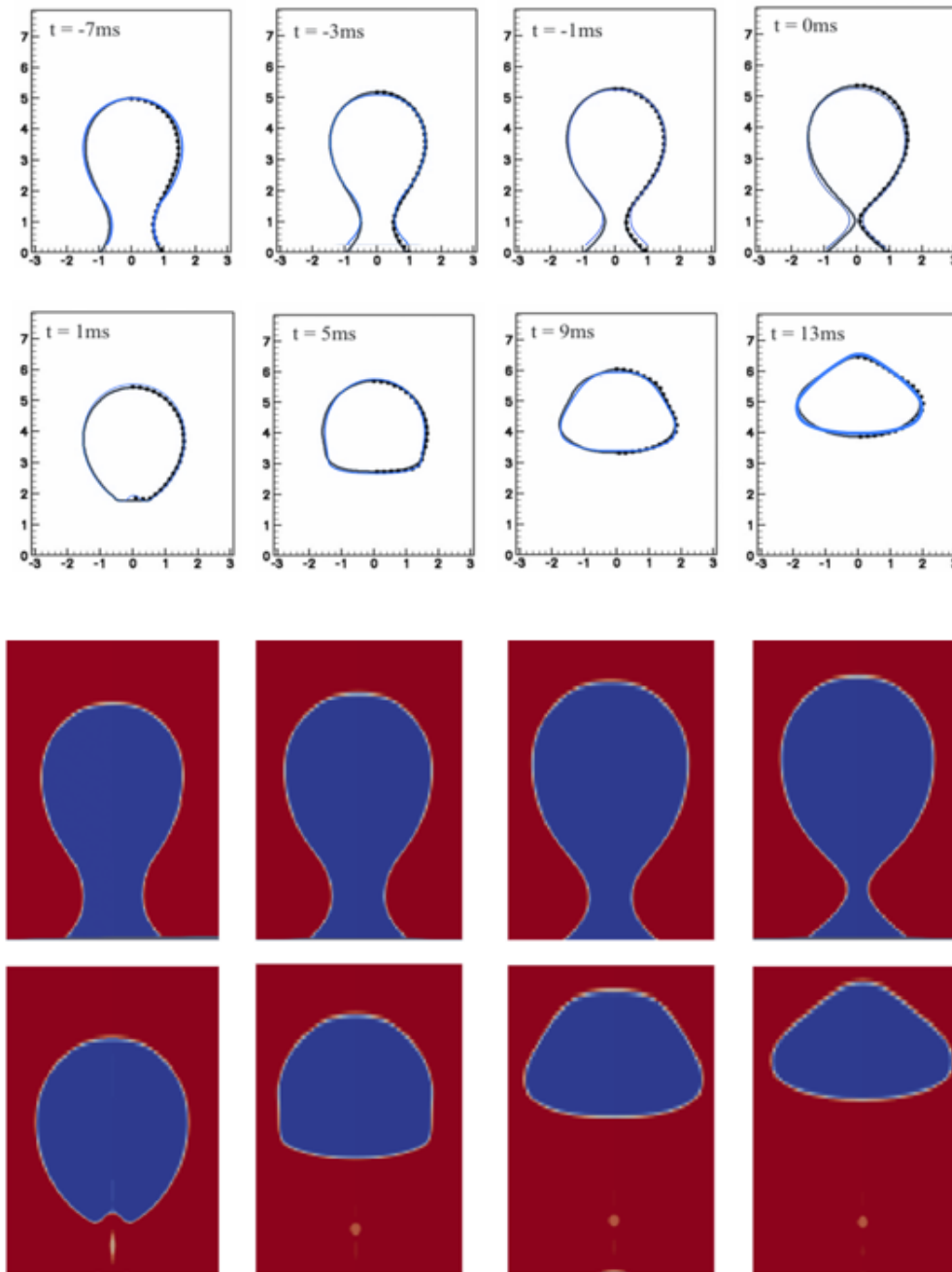


Figure 2: Validation of simulated bubble shapes for air bubble pinch-off process in water against reference data for same time steps(Overlay with reference work on top and snapshots from Open-FOAM on bottom).

7.2 Effect of Liquid Viscosity

The viscosity of the liquid phase (μ_l) is a critical parameter. We simulated cases ranging from low viscosity (4.2 cP) to high viscosity (3400 cP).

7.2.1 Bubble Formation

Figure 3 compares the temporal evolution of bubbles in liquids of increasing viscosity. At low viscosity (26 cP), the necking is rapid. As viscosity increases (68 cP to 3400 cP), viscous stresses retard the neck collapse, resulting in elongated necks and larger bubble volumes. The simulation results for the 3400 cP case deviated from the reference, while all other cases matched well. This suggests a potential limitation in the standard interFoam solver's ability to accurately resolve the quasi-static interface evolution in extremely high-viscosity regimes.

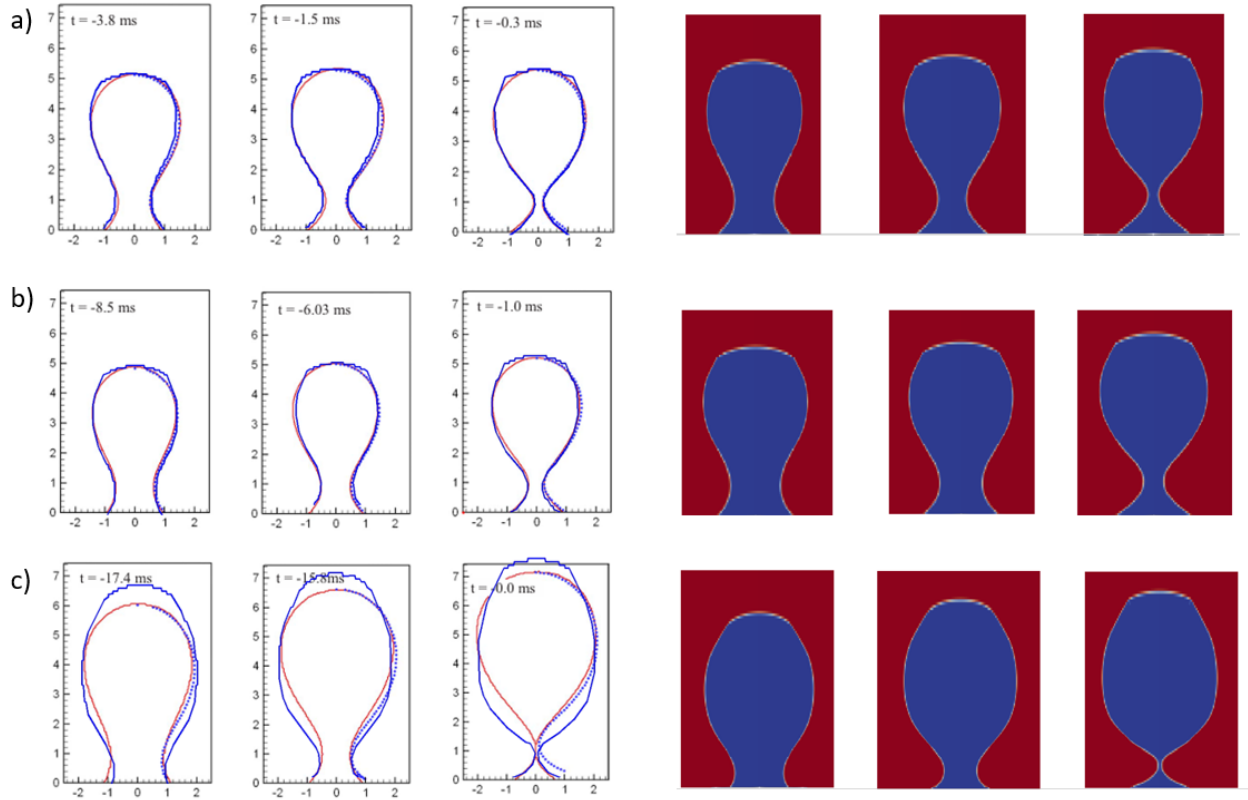


Figure 3: Bubble shapes at different viscosities: (a) 26 cP, (b) 68 cP, (c) 3400 cP. Overlay with reference work on left and snapshots from OpenFOAM on right.

7.2.2 Necking Dynamics (r vs τ)

The thinning of the neck radius r over time τ (time to pinch-off) was tracked. Figure 4 shows the detailed necking curve for the specific case of $\mu_l = 68$ cP, where the simulation data follows the reference's trend closely giving a power law exponent of 0.59.

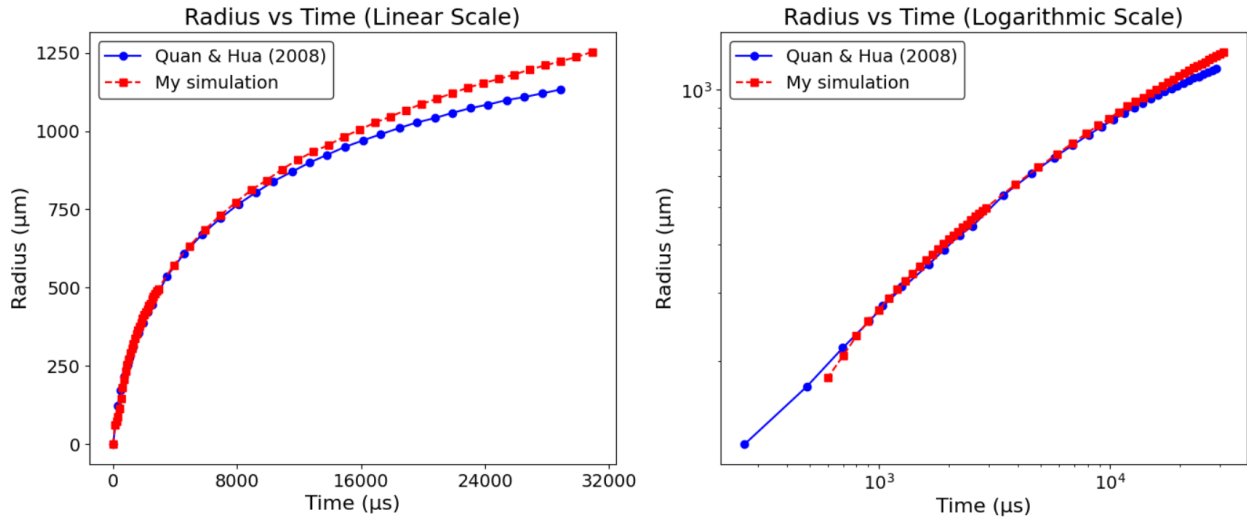


Figure 4: Detailed comparison of necking radius r vs time τ for 68 cP (Ref Fig 4).

To understand the broader trend, the necking dynamics were plotted for all viscosity variations (from 4.2 cP to 850 cP) in Figure 5. This comparison highlights how increased viscosity increases the slope of the necking curve in the log-log plot.

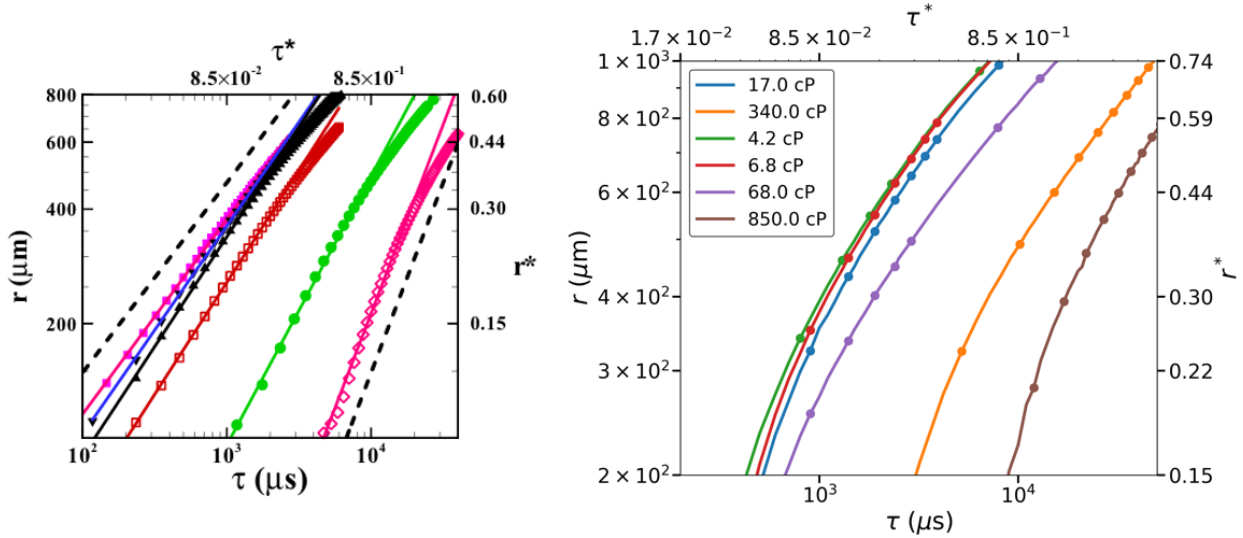


Figure 5: Necking radius (r) vs time (τ) for various liquid viscosities (Reference plot on left and our simulation's plot on right).

7.2.3 Power Law Exponent (α)

The necking process follows a power law $r \sim \tau^\alpha$. Figure 6 plots the exponent α derived from Figure 5 and plotted against viscosity. Our results show α increasing from ≈ 0.56 at low viscosity to ≈ 0.91 at high viscosity. This transition is consistent with the reference data, confirming the shift from inertia-dominated to viscous-dominated pinch-off. The simulation reproduced the reference power law exponents with a maximum deviation of approximately 9%.

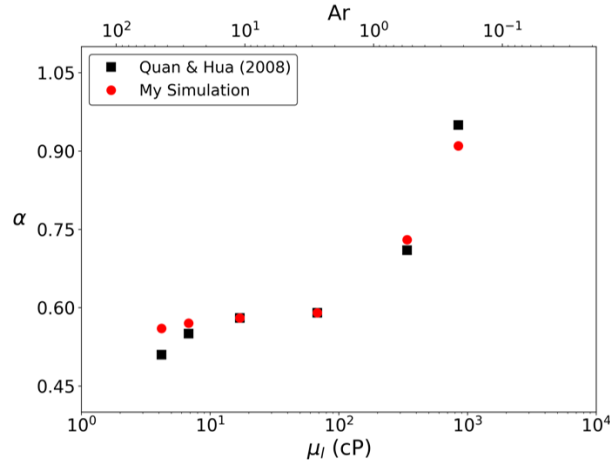
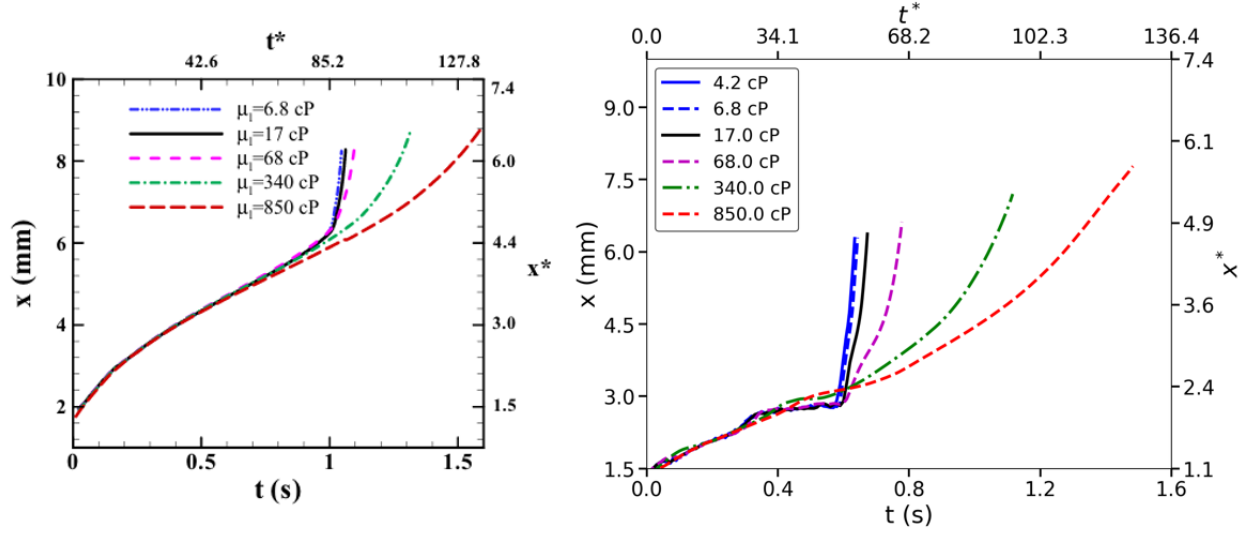


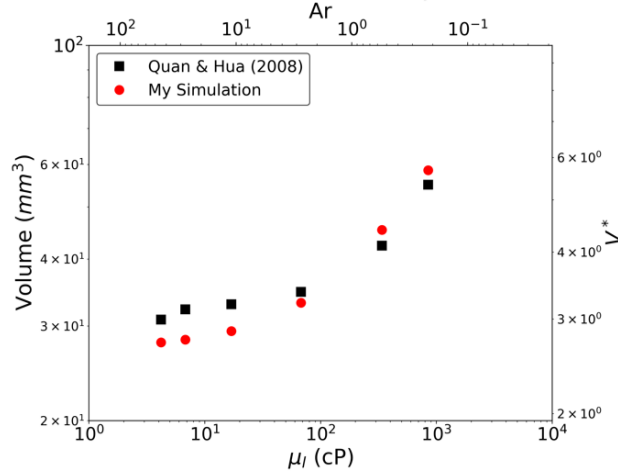
Figure 6: Variation of power-law exponent α with liquid viscosity.

7.2.4 Pinch-off Height and Bubble Volume

Viscosity also affects the vertical position of the bubble. Figure 7(a) shows the top rising distance (x) versus time. Higher viscosity significantly delays the pinch-off time. Consequently, the final bubble volume (V) increases with viscosity (Figure 7(b)), as the air flows into the bubble for a longer duration before detachment. The simulation reproduced the reference volumes with a maximum deviation of approximately 12%.



(a) Top rising distance vs time (Reference plot on left and our simulation's plot on right)



(b) Bubble volume vs Viscosity

Figure 7: Effect of viscosity on bubble rising dynamics and final volume.

7.3 Effect of Surface Tension

The surface tension (σ) was varied from 15 mN/m to 120 mN/m to study the capillary effects.

7.3.1 Necking and Power Law

Figure 8(a) displays the neck radius reduction for different surface tension values. Lower surface tension leads to faster pinch-off. The power-law exponent α derived from these curves (Figure 8(b)) shows a downward trend as surface tension increases, stabilizing around 0.6 for higher σ .

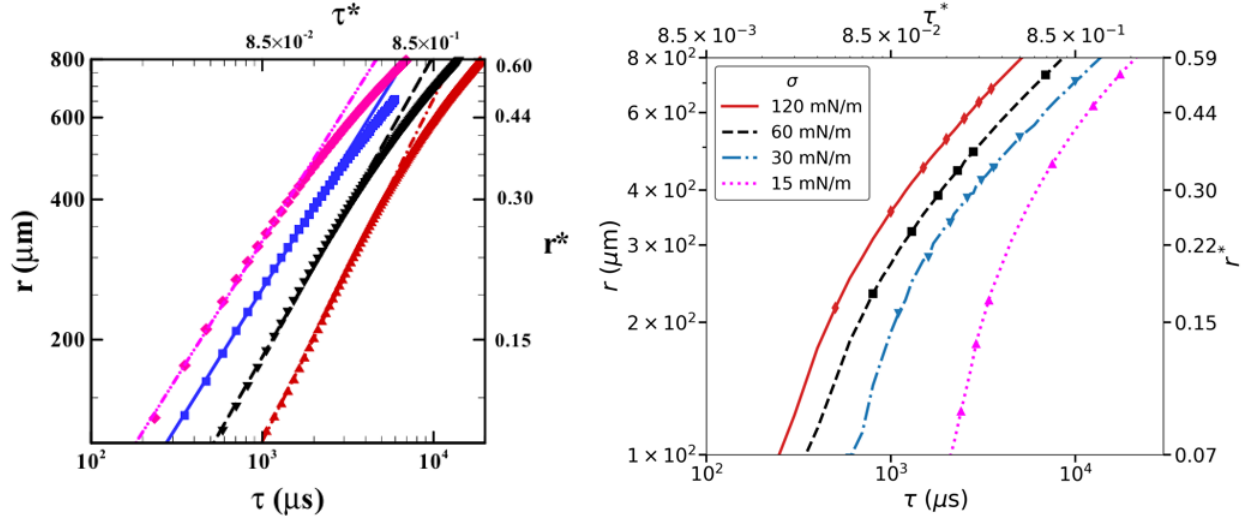
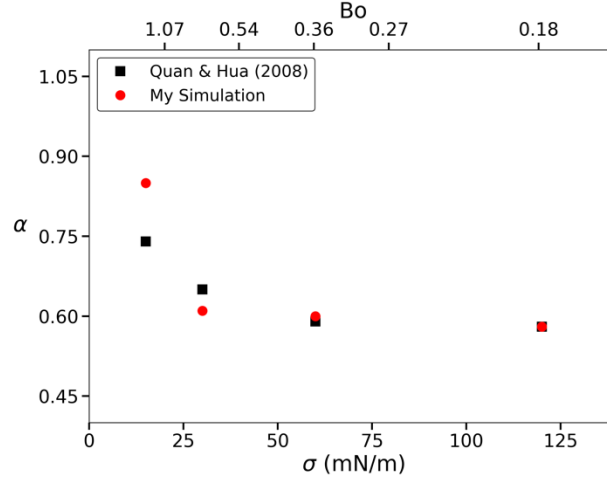
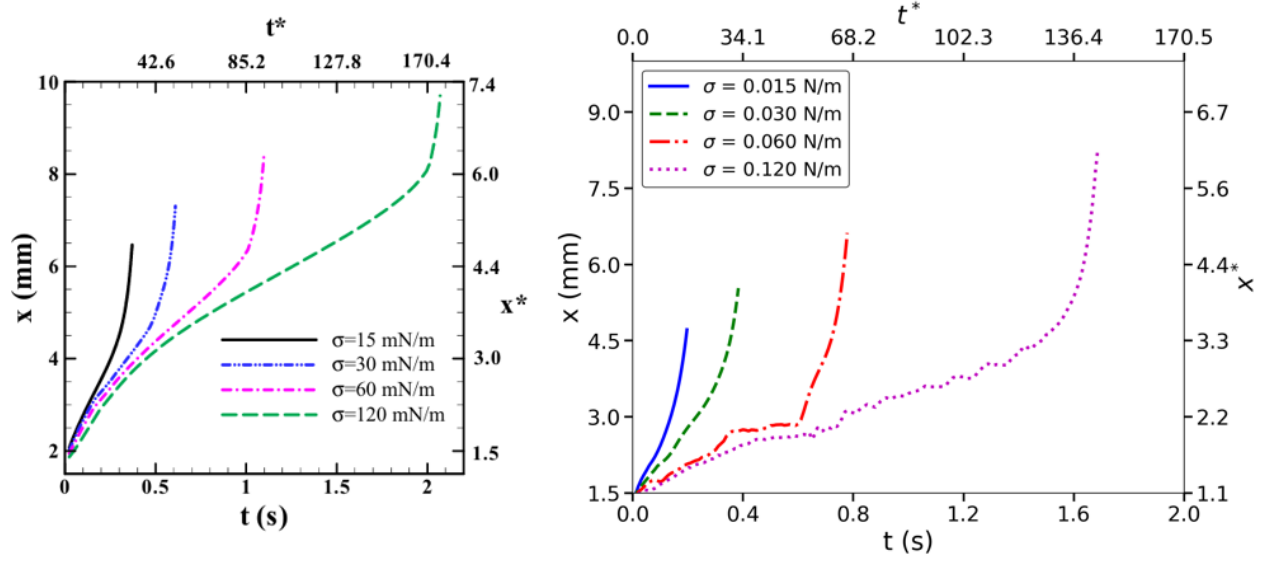
(a) r vs τ (Ref Fig 10)(b) Exponent α vs σ (Ref Fig 11)

Figure 8: Impact of surface tension on necking rates and power-law exponents.

7.3.2 Height and Volume

Increasing surface tension increases the capillary force holding the bubble to the nozzle, thereby delaying detachment (Figure 9(a)). This delay allows the bubble to grow larger. Figure 9(b) confirms a linear relationship between bubble volume and surface tension, matching the theoretical predictions and reference data within 5%.



(a) Rising distance vs time (Reference plot on left and our simulation's plot on right)

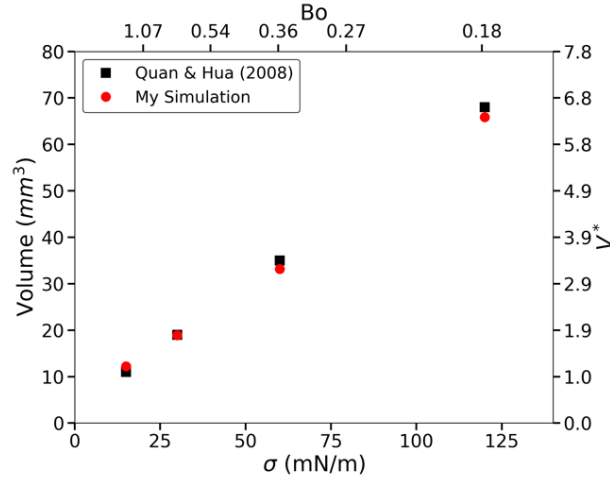
(b) Bubble volume vs σ (Ref Fig 13)

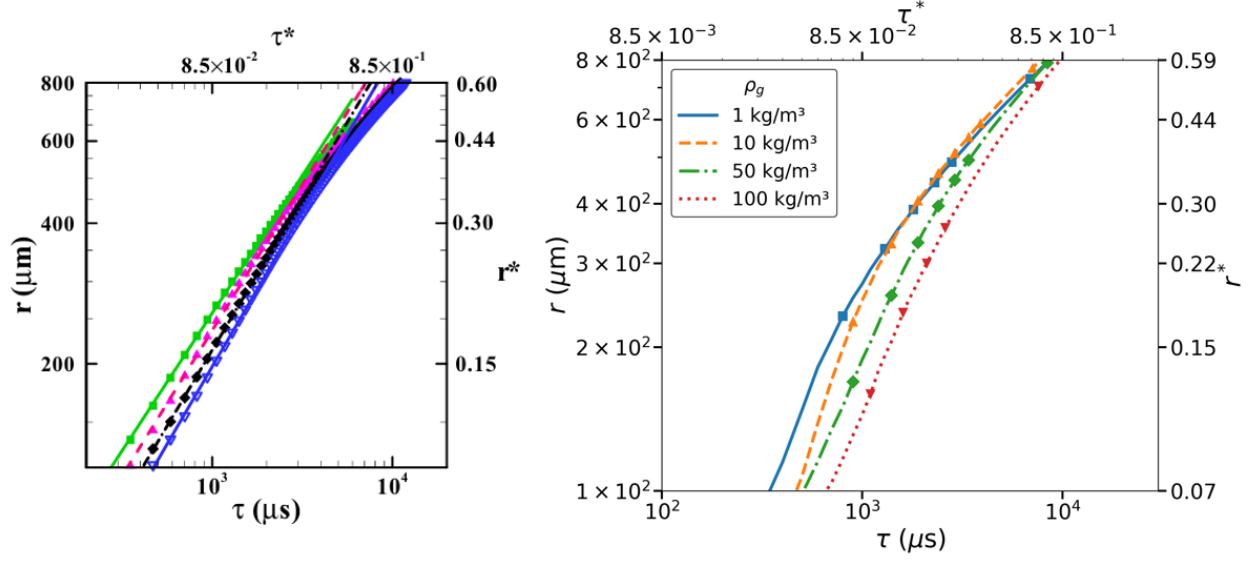
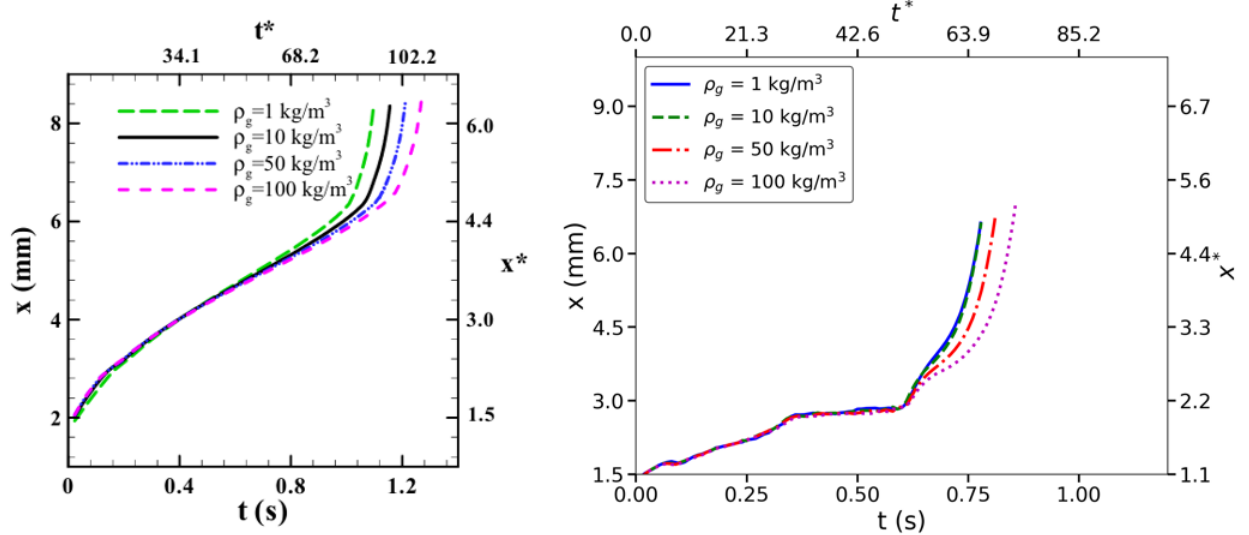
Figure 9: Effect of surface tension on rising dynamics and detachment volume.

7.4 Effect of Gas Density

Finally, the gas phase density was varied from 1 kg/m³ to 100 kg/m³.

7.4.1 Dynamics and Independence

As shown in Figure 10(a), the necking curves (r vs τ) for all density cases collapse onto a single trend. Similarly, the bubble rising distance (Figure 10(b)) shows negligible variation. This confirms that for systems with a high density ratio (liquid to gas), the inertia of the gas phase plays a minimal role in the pinch-off mechanics.

(a) r vs τ (Reference plot on left and our simulation's plot on right)

(b) Rising distance vs time (Reference plot on left and our simulation's plot on right)

Figure 10: Effect of gas density on necking and rising dynamics.

8 Conclusion

This study successfully migrated the numerical investigation of bubble necking using OpenFOAM. The simulation results demonstrate excellent agreement with the reference literature. Key findings include:

- **Viscosity:** Higher liquid viscosity delays pinch-off, increases bubble volume, and shifts the necking exponent α closer to 1.0.
- **Surface Tension:** Higher surface tension stabilizes the interface, leading to larger bubbles,

slightly lower scaling exponents and volume follows linear relation with surface tension.

- **Density:** Variations in gas density have a negligible impact on the bubble formation dynamics.

References

1. S. Quan and J. Hua, “Numerical studies of bubble necking in viscous liquids,” *Physical Review E*.
2. OpenFOAM Wiki, “InterFoam,” <https://openfoamwiki.net/index.php/InterFoam>.
3. H. N. Oguz and A. Prosperetti, “Dynamics of bubble growth and detachment from a needle,” *Journal of Fluid Mechanics*.
4. M. R. Oshaghi, H. Afshin, and B. Firoozabadi, “Investigation of bubble formation and its detachment in shear-thinning liquids at low capillary and Bond numbers,” *Theoretical and Computational Fluid Dynamics*.

DISCLAIMER: This project reproduces the results from an existing work, which has been acknowledged in the report. Any query related to the original work should not be directed to the contributor of this project.